MUSCULOSKELETAL

Diagnostic performance of electron-density dual-energy CT in detection of cervical disc herniation in comparison with standard gray-scale CT and virtual non-calcium images

Euddeum Shim[1] · Baek Hyun Kim[1] · Woo Young Kang[2] · Suk-Joo Hong[2] · Chang Ho Kang[3] · Kyung-Sik Ahn[3] · Hyeonbin Lee[2] · Thomas J. Kwack[1]

Abstract

Objectives To assess the diagnostic performance of dual-energy CT (DECT) with electron-density (ED) image reconstruction compared with standard CT (SC) and virtual non-calcium (VNCa) image CT reconstruction for detecting cervical disc herniation.
Methods This cross-sectional study was approved by the IRB. We enrolled 64 patients (336 intervertebral discs from C2/3 to C7/T1; mean age, 55 years; 17 women and 47 men) who underwent DECT with spectral reconstruction and 3-T MRI within 2 weeks between January 2018 and June 2020. Four radiologists independently evaluated the first image set of randomized SC, VNCa, and ED images to detect cervical disc herniation. After 8 weeks, the readers re-evaluated the second and the last image sets with an 8-week interval. MRI evaluations performed by two other experienced served as the reference standard. Comparing diagnostic performance between each images set was evaluated by a generalized estimating equation.
Results A total of 233 cervical disc herniations were noted on MRI. For detecting cervical disc herniation, electron-density images showed higher sensitivity (94% [219/233; 95% CI, 90–97] vs. 76% [177/233; 70–81] vs. 69% [160/233; 62–76]) ($p < 0.001$) and similar specificity (90% [93/103; 83–95] vs. 89% [92/103; 82–96] vs. 90% [93/103; 83–95]) ($p > 0.05$) as SC and VNCa images, respectively. Inter-reader agreement for cervical disc herniation calculated among the four readers was moderate for all image sets ($\kappa = 0.558$ for ED, $\kappa = 0.422$ for SC, and $\kappa = 0.449$ for VNCa).
Conclusion DECT with ED reconstruction can improve cervical disc herniation detection and diagnostic confidence compared with SC and VNCa images.
Key Points
• *Intervertebral discs with high material density are well visualized on electron-density images obtained from dual-energy CT.*
• *Electron-density images showed much higher sensitivity and diagnostic accuracy than standard CT and virtual non-calcium images for the detection of cervical disc herniation.*
• *Electron-density images can have false-negative results, especially for disc herniation with high signal intensity on T2W images and can show pseudo-disc extrusion at the lower cervical spine.*

Keywords Dual-energy computed tomography · Intervertebral disc disease · Magnetic resonance imaging · Cervical vertebrae

Abbreviations
DECT	Dual-energy CT
ED	Electron density
HU	Hounsfield units
NPV	Negative predictive value
OPLL	Ossification of posterior longitudinal ligament
PPV	Positive predictive value
SC	Standard CT
VNCa	Virtual non-calcium

✉ Baek Hyun Kim
kimbaekh@daum.net

1 Department of Radiology, Korea University Ansan Hospital, 123, Jeokgeum-ro, Danwon-gu, Ansan-si, Gyeonggi-do, Republic of Korea 15355

2 Department of Radiology, Korea University Guro Hospital, Seoul, Republic of Korea

3 Department of Radiology, Korea University Anam Hospital, Seoul, Republic of Korea

Introduction

Cervical spine CT without contrast enhancement is the primary modality to evaluate bone pathologies such as fractures or osteophytes because of its superiority over MRI [1]. However, this technique shows limited ability to reveal soft tissue lesions, including cervical disc herniation, due to its lower soft tissue contrast compared with MRI [2]. Recent studies have attempted to identify disc herniation using advanced CT technologies [3–6]. For the lumbar spine, CT shows high diagnostic performance for visualizing disc herniation [3, 4]. Notohamiprodjo et al. [3] reported that multidetector CT showed 97.8% diagnostic accuracy for evaluation of lumbar disc herniation, while Booz et al. [4] demonstrated that dual-energy CT (DECT) with virtual non-calcium (VNCa) reconstruction improved the diagnostic accuracy for depicting lumbar disc herniation by > 90% compared with standard CT (SC). However, disc herniation at the cervical spine may be more difficult to detect because of the smaller intervertebral disc, the smaller cerebrospinal fluid area with a larger spinal cord, and the beam-hardening and photon-starvation artifacts caused by the shoulder girdle [5]. The sensitivity of 64-slice multidetector CT for the detection of cervical disc herniation in 51 patients with 255 disc levels was 68% (58 of 85 herniated discs) as the reference standard assessed in 1.5-T MRI [6].

Electron-density (ED) images are obtained by converting the Hounsfield unit (HU) value of each pixel on CT images using a scanner-specific calibration curve to calculate the applied radiation dose [7]. Currently, single-source dual-layer DECT provides a more accurate ED map without conversion to HU as a calibration-free method [7]. It allows ED imaging by differentiation of Compton scattering and photoelectric effect attenuation through measurement of attenuation at two different energies [8]. Compton scattering is influenced mainly by the material density, while the ED is dependent on Compton scattering in the high-energy range, such as in radiation therapy [9, 10]. Despite the broad use of ED maps for the calculation of radiation doses in radiation oncology, this technique has not been widely used in diagnostic radiology, with one case series reporting the use of ED images to visualize lung opacity in patients with COVID-19 pneumonia [8]. We hypothesize that ED maps may show better detectability of cervical disc herniation than SC and even VNCa images of DECT since the material density of the annulus fibrosus and fibrocartilage is higher than those of the other organs [11, 12]. Moreover, ED maps may help visualize disc herniation at the lower cervical spine, which is obscured by photon-starvation and beam-hardening artifacts caused by the shoulder girdle, because these maps can reduce image noise and provide more accurate ED values in the areas with these artifacts [13].

Thus, using MRI as the reference standard, we aimed to assess the diagnostic performance and diagnostic confidence of DECT with ED reconstruction in comparison with SC and VNCa images for detecting cervical disc herniation.

Materials and methods

Our institutional review board approved this retrospective study, and the requirement for informed consent was waived.
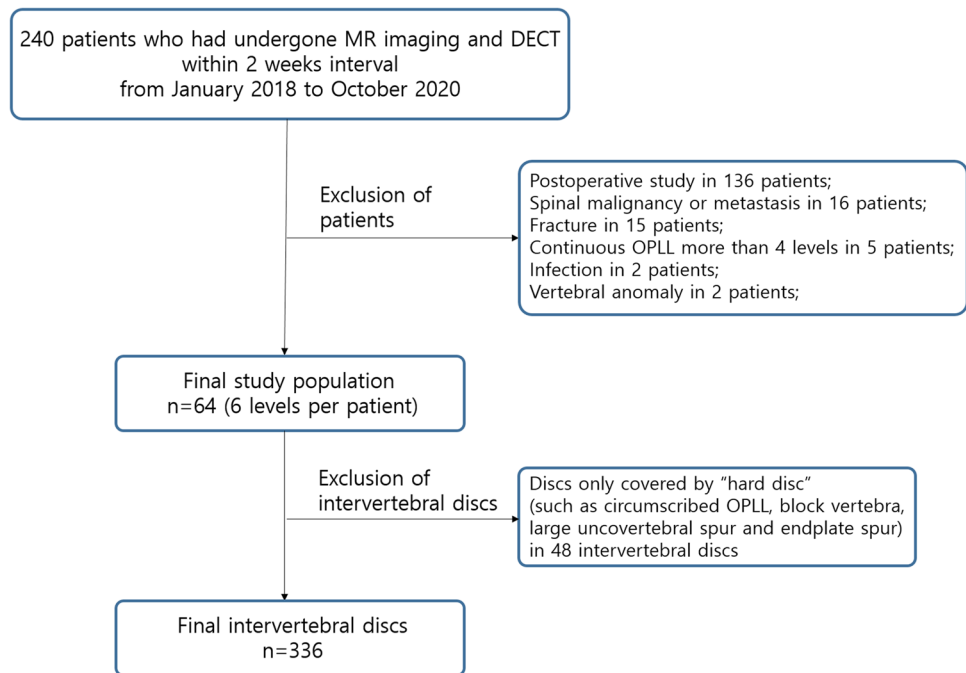
Patients

Among the 240 patients who underwent both non-contrast DECT and MRI of the cervical spine within a 2-week interval between January 2018 and June 2020, we excluded patients who underwent postoperative studies ($n = 136$) or showed spinal malignancy ($n = 16$), fracture ($n = 15$), continuous ossification of the posterior longitudinal ligament (OPLL) of more than four levels ($n = 5$), spondylodiscitis ($n = 2$), or vertebral anomalies ($n = 2$). Thus, intervertebral discs were assessed from C2/3 to C7/T1 (6 levels per patient) in 64 patients. Forty-eight intervertebral discs were excluded because they had only hard discs (such as osteophytes or OPLL) or block vertebrae. Thus, 336 cervical discs of 64 patients were evaluated (Fig. 1). The mean interval between non-contrast DECT and MRI was 2.34 days (range, 0–14 days).

Dual-energy CT protocol

All patients were scanned using a 128-slice MDCT single-source dual-layer detector spectral scanner (IQon, Philips Healthcare). All images were obtained in a craniocaudal direction from the floor of the turcica to the T2 vertebral body level. The CT scan parameters are specified in Appendix 1. Mean volume CT dose index ± standard deviation was 9.2 mGy ± 2.1 (range, 5.3–16.5 mGy) and mean dose length product was 244.6 ± 69.1 mGy·cm (range, 129.8–399.4 mGy·cm).

CT reconstruction of electron-density and virtual non-calcium images

ED and VNCa images were generated from spectral data using a commercially available advanced visualization and analysis platform (IntelliSpace Portal 10.1; Philips Healthcare). To optimize the detection of disc herniation, we sent ED and VNCa images with a visually optimized window level and width (window level and width of ED, 105 and 23; VNCa, 60 and 265) to the image viewer system. However, we allowed readers to freely adjust the window length and

Fig. 1 Flow chart for selection of the study population

width during the image assessment. The calcium suppression index of the VNCa images was fixed at 65 [14]. The slice thickness of both images was 2 mm, with an increment of 2 mm in axial and sagittal reconstruction.

MRI acquisition

All patients underwent non-contrast MRI with a 3.0-T instrument (Magnetom Skyra, Siemens Healthineers) with a dedicated spine surface coil. The MR image composition and parameters are provided in Appendix 2.

Image analysis

Image evaluation was performed with a PACS viewer solution (G3, Infinitt). First, to set the reference standard, two board-certified radiologists (7 and 19 years of experience in musculoskeletal imaging, respectively) blinded to any clinical or DECT information analyzed MRI scans in consensus to determine the presence and degree of disc herniation according to the lumbar disc pathologic classification of the North American Spine Society (version 2.0), the presence and degree of spinal stenosis, and the zone of disc herniation (Fig. 2) [15]. The definitions of disc herniation, spinal stenosis, and disc herniated zones are provided in Appendix 3. Zonal discrepancies in disc herniation were defined to an absolute value transformed by the difference between the reference zonal value and the readers' zonal value. If the T2W image showed a high signal intensity of disc herniation, it was recorded.

After defining the reference standard, four radiologists with experience in musculoskeletal imaging (two board-certified radiologists with 29 years and 10 years of experience and two radiology residents with 4 years and 1 year of experience, respectively) who were blinded to the MRI results and clinical history independently reviewed the axial and sagittal CT images. To reduce the effect of recall bias for each specific imaging set, the order of imaging assessments was set to be different for each reader (Appendix 4). Based on this order setting, each reader evaluated three CT image sets for the presence and zone of disc herniation and the grade of spinal stenosis per disc level in a randomized order, with an 8-week interval between each imaging set without any access to other image series. Assessments of diagnostic confidence and image quality, which focused on noise and imaging artifacts (such as dark streaks or photon starvation), were also performed for all CT series per disc level using five-point scales (1, unacceptable; 5, excellent).

Statistical analysis

To compare disc herniation and spinal stenosis, a generalized estimating equation with an independent correlation-working matrix and robust variance estimator to account for handling clustered data in each patient among the three CT series in a pairwise manner was performed. Data analysis was performed using the assessments obtained by each reader individually and the integrated results obtained by the four readers. The integrated results for each disc level were defined as values showing agreement among at least three of the four readers. If less than three readers showed agreement, the presence of disc herniation and spinal stenosis was determined by consensus discussion among the four
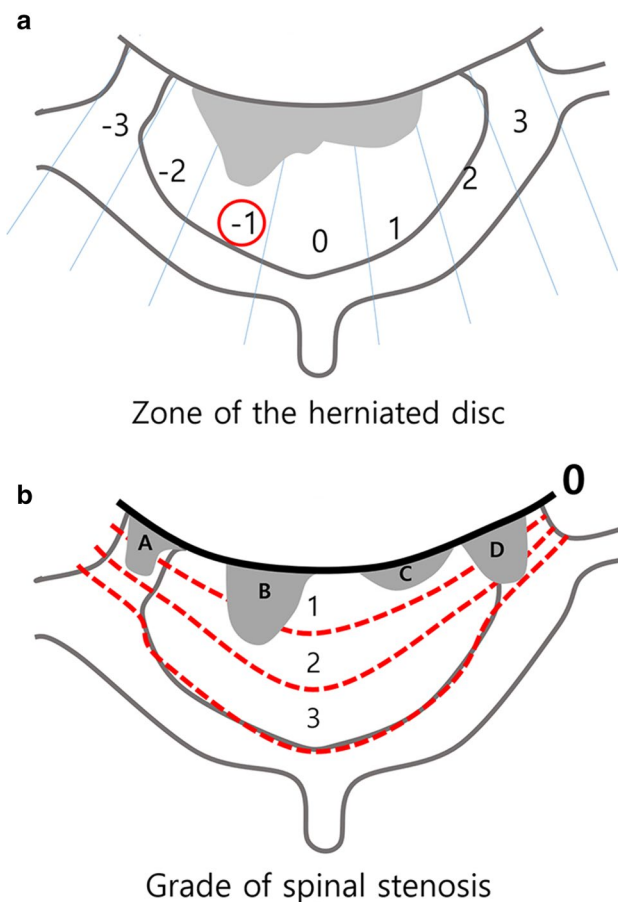
a

Zone of the herniated disc

b

Grade of spinal stenosis

Fig. 2 Schematic of the zonal distribution of the herniated disc and the grade of spinal stenosis. **a**, The central canal is divided by the inner margin of both pedicles and is evenly divided into five zones (−2, right subarticular; −1, right central; 0, central; 1, left central; 2, left subarticular). Two additional zones were defined as the foraminal zones from the inner to the outer margins of both pedicles (−3, right foraminal; 3, left foraminal). **b**, For spinal stenosis, the location of the posterior margin of the largest herniated disc was categorized into three grades on the basis of the anterior-to-posterior length of the spinal canal

readers. The sensitivity, specificity, negative predictive value (NPV), and positive predictive value (PPV) of each method were calculated using 2×2 contingency tables. Linear mixed model statistics were used to analyze the zonal discrepancies among the three CT series. Comparison of variables at the same disc level was performed using the McNemar test (for sensitivity and specificity per disc level) and Wilcoxon signed-rank test (for diagnostic confidence and image quality). Regarding the presence of cervical disc herniation and spinal stenosis, inter-reader agreements among the four readers were measured using Fleiss κ [16, 17]. Kappa results were qualitatively stratified by score κ = 0.81–1.00, (almost) perfect agreement; κ = 0.61–0.80, substantial agreement; κ = 0.41–0.60, moderate agreement; κ = 0.21–0.40, fair agreement; and κ and .20, slight agreement [17]. Statistical analyses were performed using SPSS version 26 (IBM

Corporation) and MedCalc version 16.4.1 (MedCalc Software). $p < 0.05$ was considered statistically significant.

Results

A total of 336 intervertebral discs in 64 patients (47 men and 17 women; mean age, 55 ± 12.9 [SD] years; range, 25–85 years; mean body mass index, 25.9 ± 3.48 [SD]) were finally included. Among the 336 intervertebral discs, 233 (69.3%) showed disc herniation on MRI: 127 protrusions and 106 extrusions. A total of 103 discs (30.7%), including 80 normal and 23 bulging discs, showed no disc herniation. Grade 2 or 3 spinal stenosis was observed in 50 of the 233 herniated intervertebral discs (21.5%). The distribution of disc herniations according to the disc level was as follows: C2/3, 21 disc herniations; C3/4, 43; C4/5, 51; C5/6, 50; C6/7, 45; C7/T1, 23. The disc herniations were recorded in the right foraminal zone (denoted as −3) in 4 discs, right subarticular zone (−2) in 14 discs, right central zone (−1) in 5 discs, central zone (0) in 134 discs, left central zone (1) in 42 discs, left subarticular zone (2) in 20 discs, and left foraminal zone (3) in 14 discs. Two intervertebral disc herniations showed a high signal intensity on T2W images.

Diagnostic performance for cervical disc herniation and spinal stenosis

The diagnostic performance for cervical disc herniation was summarized by integrating the assessments performed by the four readers (Table 1) and by evaluating each reader's assessments individually (Table 2). The diagnostic accuracy of ED images for disc herniation was much higher than those for SC and VNCa images, regardless of readers ($p < 0.001$) (Table 2). All readers showed significantly better sensitivity with ED images (Table 2 and Fig. 3). However, the specificity of ED images was lower than that of SC and VNCa images in assessments by reader 1 and VNCa images in assessments by reader 3 (Table 2). The diagnostic accuracy of disc herniation was not different between SC and VNCa images ($p > 0.05$), except for reader 3 (the p values for sensitivity, specificity, and accuracy are provided in Supplemental Table 2).

For spinal stenosis assessment, all readers showed significantly better sensitivity with the ED map (Table 2). Although the specificity of ED images was lower than VNCa images in assessments by reader 1 ($p < 0.05$), the differences were not significant in assessments by other readers (Table 2 and supplemental Table 2). Inter-reader agreement for cervical disc herniation, calculated among all four readers, was moderate for all image sets; slightly higher for ED images (κ = 0.558) than for SC (κ = 0.422) and VNCa (κ = 0.449) images. Inter-reader agreement for spinal stenosis was moderate for all image sets, too, higher for ED images (κ = 0.571) than for SC (κ = 0.392) and VNCa (κ = 0.387) images.

Table 1 Comparison of the diagnostic accuracy for cervical disc herniation and extrusion as well as spinal stenosis on standard CT (SC), virtual non-calcium (VNCa), and electron-density (ED) images per intervertebral disc based on integrated data

	Sensitivity[a]	Specificity[a]	Negative predictive value	Positive predictive value	Accuracy[a]	p (SC-VNCa)[b]	p (VNCa-ED)[b]	p (SC-ED)[b]
Cervical disc herniation								
SC	**76 (177/233)[c]** [70, 81]	89 (92/103) [82, 96]	62 (92/148) [56, 68]	94 (177/188) [90, 97]	**80 (269/336)[c]** [75, 84]	0.076	< 0.001	< 0.001
VNCa	**69 (160/233)[c]** [62, 76]	90 (93/103) [83, 95]	56 (93/166) [51, 61]	94 (160/170) [90, 97]	**75 (253/336)[c]** [70, 80]			
ED	**94 (219/233)** [90, 97]	90 (93/103) [83, 95]	87 (93/107) [80, 92]	96 (219/229) [92, 98]	**93 (312/336)** [90, 95]			
Cervical disc extrusion								
SC	**68 (72/106)[c]** [58, 77]	**89 (205/230)[c]** [84, 93]	86 (205/239) [82, 89]	74 (72/97) [66, 81]	82 (277/336) [78, 86]	0.541	< 0.001	< 0.001
VNCa	**60 (64/106)[c]** [50, 70]	**88 (202/230)[c]** [83, 92]	83 (202/244) [79, 86]	70 (64/92) [61, 77]	79 (266/336) [74, 83]			
ED	**90 (95/106)** [82, 95]	**77 (176/230)** [71, 82]	94 (176/187) [90, 97]	64 (95/149) [58, 69]	81 (271/336) [76, 85]			
Spinal stenosis (grade 2 or more)								
SC	70 (35/50) [55, 82]	93 (267/286) [90, 96]	95 (267/282) [92, 96]	65 (35/54) [53, 75]	90 (302/336) [86, 93]	0.408	0.325	0.039
VNCa	72 (36/50) [58, 84]	92 (263/286) [88, 95]	95 (263/277) [92, 97]	61 (36/59) [50, 71]	89 (299/336) [85, 92]			
ED	80 (40/50) [66, 90]	92 (262/286) [88, 95]	96 (262/272) [94, 98]	63 (40/64) [53, 71]	90 (302/336) [86, 93]			

Note—Unless otherwise specified, data are percentages, and the numbers in parentheses are the numbers of patients used to calculate the percentage values. Data in brackets are 95% confidence intervals

[a] p-values for sensitivity, specificity, and accuracy were calculated by the generalized estimating equation method, and the individual values are presented in supplemental Table 1

[b] p-values noted in the table were obtained for 336 intervertebral discs using three imaging methods and calculated by the generalized estimated equation method in a pairwise manner

[c] The data in bold text are values showing statistically significant differences between the imaging method and the electron-density map. The individual p-values are presented in supplemental Table 1

Reduced diagnostic performance for disc herniation at the C7/T1 level

The sensitivity and specificity of disc herniation assessments according to disc levels are shown in Table 3. The disc-level sensitivity of disc herniation assessments was likely to be higher in the ED images than in the SC and VNCa images for all readers. All readers showed a considerable reduction in sensitivity at the C7/T1 level on the three CT image series, but the sensitivity on the ED map was still significantly higher than that on SC and VNCa images (Table 3; individual p-values are provided in Supplemental Table 3). Specificity did not differ according to the imaging series, except at the C2/3 level in assessments by readers 1 and 3 (Table 3).

Zonal discrepancies in disc herniation

The mean zonal discrepancy was 1 or less for all image types (Table 4), with the highest values recorded on VNCa images

for readers 2, 3, and 4 and on SC images for reader 1. The zonal discrepancy on the ED map was lower than that of the VNCa map for all readers (statistically significant only for reader 2) and lower than that on SC images for readers 1 and 2 ($p > 0.05$).

Diagnostic confidence and image-quality assessments

For diagnosis of cervical disc herniation, ED images showed significantly higher diagnostic confidence and image quality than SC and VNCa images at all cervical disc levels (all $p < 0.001$) (Fig. 4). SC images showed higher diagnostic confidence and image quality than VNCa images at all disc levels (all $p < 0.001$). Both diagnostic confidence and image quality tended to decrease at C6/7 and C7/T1 disc levels, being lowest at the C7/T1 level in all three imaging sets (mean scores and standard deviations are reported in Supplemental Table 3) (Fig. 4).

Table 2 Comparison of the diagnostic accuracies of all readers for the detection of cervical disc herniation per intervertebral disc

	Sensitivity[a]	Specificity[a]	Negative predictive value	Positive predictive value	Accuracy[a]	p (SC-VNCa)[b]	p (VNCa-ED)[b]	p (SC-ED)[b]
Disc herniation								
Reader 1								
SC	**44 (102/233)[c]** [37, 80]	**85 (88/103)[c]** [77, 92]	40 (88/219) [37, 44]	87 (102/117) [81, 92]	**57 (190/336)[c]** [51, 62]	0.610	< 0.001	< 0.001
VNCa	**44 (102/233)[c]** [37, 50]	**91 (94/103)[c]** [84, 96]	42 (94/225) [39, 45]	92 (102/111) [86, 96]	**58 (196/336)[c]** [53, 64]			
ED	**82 (190/233)** [76, 86]	**71 (73/103)** [61, 79]	63 (73/116) [56, 70]	86 (190/220) [82, 90]	**78 (263/336)** [73, 83]			
Reader 2								
SC	**64 (149/233)[c]** [57, 70]	79 (81/103) [69, 86]	49 (81/165) [44, 54]	87 (149/171) [82, 91]	**68 (230/336)[c]** [63, 73]	0.379	0.002	< 0.001
VNCa	**66 (153/233)[c]** [59, 72]	75 (77/103) [95, 83]	49 (77/157) [44, 54]	86 (153/179) [81, 89]	**68 (230/336)[c]** [63, 73]			
ED	**78 (182/233)** [72, 83]	75 (77/103) [65, 83]	60 (77/128) [54, 66]	88 (182/208) [72, 91]	**77 (259/336)** [72, 81]			
Reader 3								
SC	**73 (170/233)[c]** [67, 79]	84 (86/103) [75, 90]	58 (86/149) [52, 63]	91 (170/187) [87, 94]	**76 (256/336)[c]** [71, 81]	< 0.001	< 0.001	< 0.001
VNCa	**61 (143/233)[c]** [55, 68]	**92 (95/103)[c]** [85, 97]	51 (95/185) [47, 56]	95 (143/151) [90, 97]	**71 (238/336)[c]** [66, 76]			
ED	**91 (213/233)** [87, 95]	**83 (85/103)** [74, 89]	81 (85/105) [73, 87]	92 (213/231) [89, 95]	**89 (298/336)** [85, 92]			
Reader 4								
SC	**69 (161/233)[c]** [63, 75]	85 (87/103) [76, 91]	55 (87/159) [50, 60]	91 (161/177) [69, 78]	**74 (248/336)[c]** [69, 78]	0.347	< 0.001	< 0.001
VNCa	**71 (165/233)[c]** [63, 75]	80 (82/103) [76, 91]	55 (82/150) [50, 60]	89 (165/186) [86, 94]	**74 (247/336)[c]** [69, 78]			
ED	**90 (209/233)** [85, 93]	86 (89/103) [78, 92]	79 (89/113) [72, 85]	94 (209/223) [90, 96]	**89 (298/336)** [85, 92]			
Spinal stenosis								
Reader 1								
SC	**30 (15/50)[c]** [18, 45]	92 (262/286) [88, 95]	88 (262/297) [86, 90]	38 (15/39) [26, 53]	82 (277/336) [78, 86]	0.146	< 0.001	0.028
VNCa	**28 (14/50)[c]** [16, 42]	**97 (277/286)[c]** [94, 99]	89 (277/282) [87, 90]	61 (14/23) [42, 77]	87 (291/336) [82, 90]			
ED	**58 (29/50)** [28, 57]	**90 (257/286)** [86, 93]	92 (257/278) [87, 92]	50 (29/58) [31, 54]	85 (286/336) [78, 87]			
Reader 2								
SC	**44 (22/50)[c]** [30, 59]	92 (263/286) [88, 95]	90 (263/291) [88, 92]	49 (22/45) [37, 61]	**85 (285/336)[c]** [81, 88]	0.176	0.743	0.207
VNCa	**52 (26/50)[c]** [37, 66]	90 (257/286) [86, 93]	92 (257/281) [89, 93]	47 (26/55) [37, 57]	**84 (283/336)[c]** [80, 88]			
ED	**64 (32/50)** [49, 77]	93 (266/286) [89, 96]	94 (266/284) [91, 96]	62 (32/52) [50, 72]	**89 (298/336)** [85, 92]			
Reader 3								
SC	**62 (31/50)[c]** [47, 75]	86 (247/286) [82, 90]	93 (274/266) [90, 95]	44 (31/70) [36, 53]	83 (278/336) [78, 87]	0.687	0.033	0.186
VNCa	**62 (31/50)[c]** [47, 75]	87 (250/286) [83, 91]	93 (250/269) [90, 95]	46 (31/67) [37, 56]	84 (281/336) [79, 87]			
ED	**82 (41/50)** [69, 91]	87 (248/286) [82, 90]	97 (248/286) [94, 98]	52 (41/79) [44, 60]	86 (289/336) [82, 90]			

Table 2 (continued)

	Sensitivity[a]	Specificity[a]	Negative predictive value	Positive predictive value	Accuracy[a]	p (SC-VNCa)[b]	p (VNCa-ED)[b]	p (SC-ED)[b]
Reader 4								
SC	**74 (37/50)[c]** [60, 85]	87 (249/286) [83, 91]	95 (249/262) [92, 97]	50 (37/74) [42, 58]	85 (286/336) [81, 89]	0.273	0.452	0.037
VNCa	**66 (33/50)[c]** [51, 79]	84 (239/286) [78, 88]	93 (239/256) [90, 95]	41 (33/80) [34, 49]	**81 (272/336)[c]** [76, 85]			
ED	**84 (42/50)** [71, 93]	85 (243/286) [81, 89]	97 (243/251) [84, 98]	49 (42/85) [42, 57]	**85 (285/336)** [81, 88]			

SC, standard CT image; *VNCa*, virtual non-calcium image; *ED*, electron-density image

Note—Unless otherwise specified, data are percentages, and the numbers in parentheses are the numbers of patients used to calculate the percentage values. Data in brackets are the 95% confidence intervals

[a]*p*-values for sensitivity, specificity, and accuracy were calculated by the generalized estimating equation method, and the individual values are presented in supplemental Table 2

[b]*p*-values noted in the table were obtained for 336 intervertebral discs by using three imaging methods and calculated by the generalized estimated equation method in a pairwise manner

[c]The data in bold text are values showing statistically significant differences between the imaging method and the electron-density map. The individual *p*-values are presented in supplemental Table 2

False-negative and false-positive findings on ED images

The integrated ED results of the four readers yielded 14 false-negative (C2/3, 1; C3/4, 1; C4/5, 1; C5/6, 2; C6/7, 5; and C7/T1, 4) and 10 false-positive (C2/3, 4; C3/4, 1; C6/7, 3; and C7/T1, 2) findings for intervertebral discs. Among the 14 false-negative lesions, two were large disc herniations showing high signal intensity on T2W images at C3/4 and C7/T1 levels (Fig. 5). None of the four readers found the lesion at C3/4, and the most experienced reader only found disc herniation at C7/T1 (Fig. 5). None of the readers found T2 high signal disc herniation on SC and VNCa maps. A pseudo-disc herniation mimicking a large extrusion was
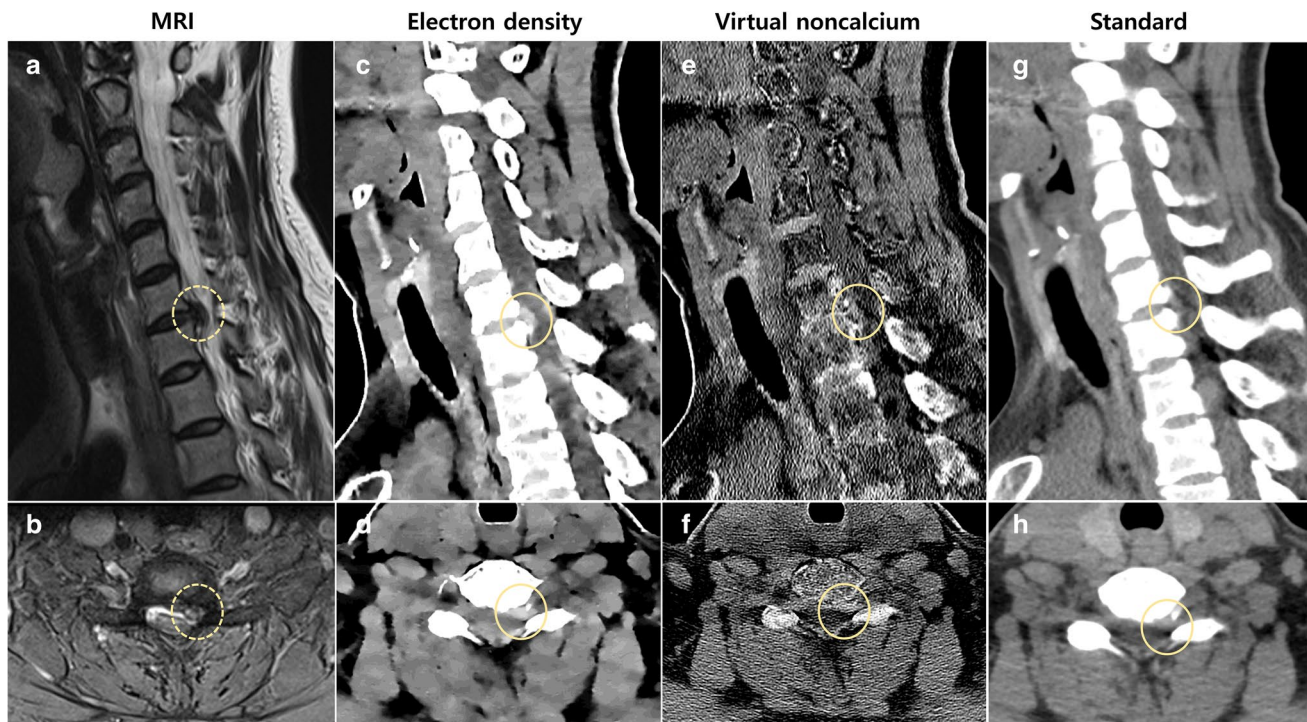

Fig. 3 A 48-year-old female with radiating pain to the left upper extremity. **a, b** T2-weighted sagittal image (**a**) and T2-weighted fat-suppressed axial image (**b**) show disc extrusion at the left subarticular and foraminal zones. **c–h**, Electron-density images (**c, d**) more clearly demonstrate disc herniation (circles), in comparison with virtual non-calcium images (**e, f**) and standard images (**g, h**)

Table 3 Sensitivity (Sn) and specificity (Sp) of cervical disc herniation according to the disc level and readers

	C2/3 Sn[a]	C2/3 Sp[a]	C3/4 Sn[a]	C3/4 Sp[a]	C4/5 Sn[a]	C4/5 Sp[a]	C5/6 Sn[a]	C5/6 Sp[a]	C6/7 Sn[a]	C6/7 Sp[a]	C7/T1 Sn[a]	C7/T1 Sp[a]
Reader 1												
SC	**33 (7/21)[b]** [15, 57]	**88 (29/33)[b]** [72, 97]	**40 (17/43)[b]** [25, 56]	77 (10/13) [46, 95]	**51 (26/51)[b]** [37, 65]	78 (7/9) [40, 97]	**68 (34/50)[b]** [53, 80]	25 (1/4) [1, 81]	**33 (15/45)[b]** [20, 49]	88 (7/8) [47, 100]	**9 (2/23)[b]** [1, 28]	92 (33/36) [78, 98]
VNCa	**33 (7/21)[b]** [15, 57]	**88 (29/33)[b]** [72, 97]	**56 (24/43)[b]** [40, 71]	77 (10/13) [46, 95]	**49 (25/51)[b]** [35, 63]	89 (8/9) [52, 100]	**60 (30/50)[b]** [45, 74]	100 (4/4) [40, 100]	**33 (15/45)[b]** [20, 49]	100 (8/8) [63, 100]	**9 (2/23)[b]** [1, 28]	100 (36/36) [90, 100]
ED	86 (18/21) [64, 97]	55 (18/33) [36, 72]	91 (39/43) [78, 97]	69 (9/13) [39, 91]	90 (46/51) [79, 97]	56 (5/9) [21, 86]	88 (44/50) [76, 95]	75 (3/4) [19, 99]	73 (33/45) [58, 85]	50 (4/8) [16, 84]	44 (10/23) [23, 66]	94 (34/36) [81, 99]
Reader 2												
SC	81 (17/21) [58, 95]	49 (16/33) [31, 66]	**70 (30/43)[b]** [30, 53]	85 (11/13) [55, 98]	**59 (30/51)[b]** [44, 72]	89 (8/9) [52, 100]	60 (30/50) [45, 74]	25 (1/4) [1, 81]	71 (32/45) [56, 84]	88 (7/8) [47, 100]	**35 (8/23)[b]** [16, 57]	100 (36/36) [90, 100]
VNCa	86 (18/21) [64, 97]	58 (19/33) [39, 75]	77 (33/43) [61, 88]	85 (11/13) [55, 98]	67 (34/51) [52, 79]	78 (7/9) [40, 97]	70 (35/50) [55, 82]	75 (3/4) [19, 99]	60 (27/45) [44, 74]	63 (5/8) [24, 91]	**26 (6/23)[b]** [10, 97]	89 (32/36) [74, 97]
ED	91 (19/21) [70, 99]	58 (19/33) [39, 75]	93 (40/43) [81, 99]	62 (8/13) [32, 86]	78 (40/51) [65, 89]	78 (7/9) [40, 97]	74 (37/50) [60, 85]	75 (3/4) [19, 99]	76 (34/45) [60, 87]	75 (6/8) [35, 97]	48 (11/23) [27, 69]	92 (33/36) [78, 98]
Reader 3												
SC	86 (18/21) [64, 97]	73 (24/33) [54, 87]	**72 (31/43)[b]** [56, 85]	69 (9/13) [39, 91]	86 (44/51) [74, 94]	89 (8/9) [52, 100]	84 (42/50) [71, 93]	75 (3/4) [19, 99]	**69 (31/45)[b]** [53, 82]	100 (8/8) [63, 100]	**17 (4/23)[b]** [5, 39]	94 (34/36) [81, 99]
VNCa	**62 (13/21)[b]** [38, 82]	**97 (32/33)[b]** [84, 100]	**74 (32/43)[b]** [59, 86]	85 (11/13) [55, 98]	**77 (39/51)[b]** [63, 87]	89 (8/9) [52, 100]	**76 (38/50)[b]** [62, 87]	75 (3/4) [19, 99]	**40 (18/45)[b]** [26, 56]	75 (6/8) [35, 97]	**13 (3/23)[b]** [3, 34]	97 (35/36) [85, 100]
ED	91 (19/21) [70, 99]	76 (25/33) [58, 89]	91 (39/43) [78, 97]	85 (11/13) [55, 98]	94 (48/51) [84, 99]	89 (8/9) [52, 100]	94 (47/50) [83, 99]	75 (3/4) [19, 99]	89 (40/45) [76, 91]	63 (5/8) [24, 91]	83 (19/23) [61, 95]	49 (32/36) [74, 97]
Reader 4												
SC	**57 (12/21)[b]** [34, 78]	82 (27/33) [65, 93]	**60 (26/43)[b]** [44, 75]	85 (11/13) [55, 98]	**68 (39/51)[b]** [63, 87]	78 (7/9) [40, 97]	86 (43/50) [73, 94]	75 (3/4) [19, 99]	80 (36/45) [65, 90]	63 (5/8) [24, 91]	**26 (6/23)[b]** [10, 48]	97 (35/36) [85, 100]
VNCa	62 (13/21) [38, 82]	76 (22/33) [48, 82]	**72 (31/43)[b]** [56, 85]	85 (11/13) [55, 98]	78 (40/51) [65, 89]	67 (6/9) [30, 93]	86 (43/50) [73, 94]	75 (3/4) [19, 99]	**67 (30/45)[b]** [51, 80]	50 (4/8) [16, 84]	**35 (8/23)[b]** [16, 57]	92 (33/36) [78, 98]
ED	86 (18/21) [64, 97]	88 (29/33) [72, 97]	91 (39/43) [78, 97]	92 (12/13) [64, 100]	82 (47/51) [81, 98]	78 (7/9) [40, 97]	92 (46/50) [81, 98]	75 (3/4) [19, 99]	91 (41/45) [79, 98]	50 (4/8) [16, 84]	83 (19/23) [61, 95]	94 (34/36) [81, 99]

SC, standard CT image; *VNCa*, virtual non-calcium image; *ED*, electron-density image

Note—Unless otherwise specified, data are percentages, and the numbers in parentheses are the numbers of patients used to calculate the percentage values. Data in brackets are 95% confidence intervals

[a]Each p-value for sensitivity and specificity was calculated by McNemar test, and the individual values are presented in supplemental Table 3

[b]The data in bold text are values showing statistically significant differences between the imaging method and the electron-density map. The individual *p*-values are presented in supplemental Table 3

Table 4 Comparison of zonal discrepancies in disc herniation

	SC	VNCa	ED	p (SC-VNCa)[a]	p (VNCa-ED)[a]	p (ED-SC)[a]
Average	0.578 (0.734)	0.633 (0.779)	0.521 (0.718)	0.125	0.003	0.159
Reader 1	0.828 (1.204)	0.655 (0.999)	0.584 (0.971)	0.010	0.100	0.316
Reader 2	0.577 (0.838)	0.733 (0.984)	0.557 (0.894)	0.007	0.003	0.916
Reader 3	0.459 (0.792)	0.545 (0.920)	0.459 (0.877)	0.090	0.092	0.813
Reader 4	0.447 (0.740)	0.600 (0.954)	0.482 (0.808)	0.007	0.738	0.012

SC, standard CT image; *VNCa*, virtual non-calcium image; *ED*, electron-density image

Note—Unless otherwise specified, data are mean ± SD values

[a]Differences among imaging methods were evaluated using the linear mixed model

observed in three intervertebral discs: two at C6/7 and one at C7/T1 (Fig. 6). Other false-negative or false-positive lesions showed minimal disc protrusion or bulging discs on MR images and were negligible lesions without spinal stenosis.

Discussion

In our study, the ED map showed better sensitivity than SC and VNCa images for detection of cervical disc herniation. On SC images, the sensitivity and specificity of cervical disc herniation were 76% and 89%, respectively, similar to those reported using multidetector CT scans by Yi et al. [6]. However, the sensitivity of ED images was 94%. Human cartilage tissue, including intervertebral discs, shows higher density (range: 1.07–1.101 g·cm^{-3}) than muscle and many other organs (range: 1.00–1.07 g·cm^{-3}) [17]. Considering the high correlation between mass density and ED, intervertebral discs would be better visualized on ED images [17]. The specificity of ED images was lower than those on SC and VNCa images in assessments by readers 1 and 3. It may be because the NPV of SC and VNCa images were much lower than those of ED images. ED images showed much better NPV than SC and VNCa images in assessments by readers 1 and 3. Thus, ED maps may have the potential to improve the detection of any structure or disease for visualization of different mass densities in diagnostic radiology [8, 18]. In our experience, the costal cartilage as well as the intervertebral discs was well-observed on ED images. ED images are believed to be helpful in

Fig. 4 Line graphs of image quality (**a**) and diagnostic confidence (**b**) on standard CT, virtual non-calcium images, and electron-density images by disc levels. The mean score of image quality and diagnostic confidence decreased at C7/T1. However, the score on electron-density images was significantly higher than those on standard and virtual non-calcium images
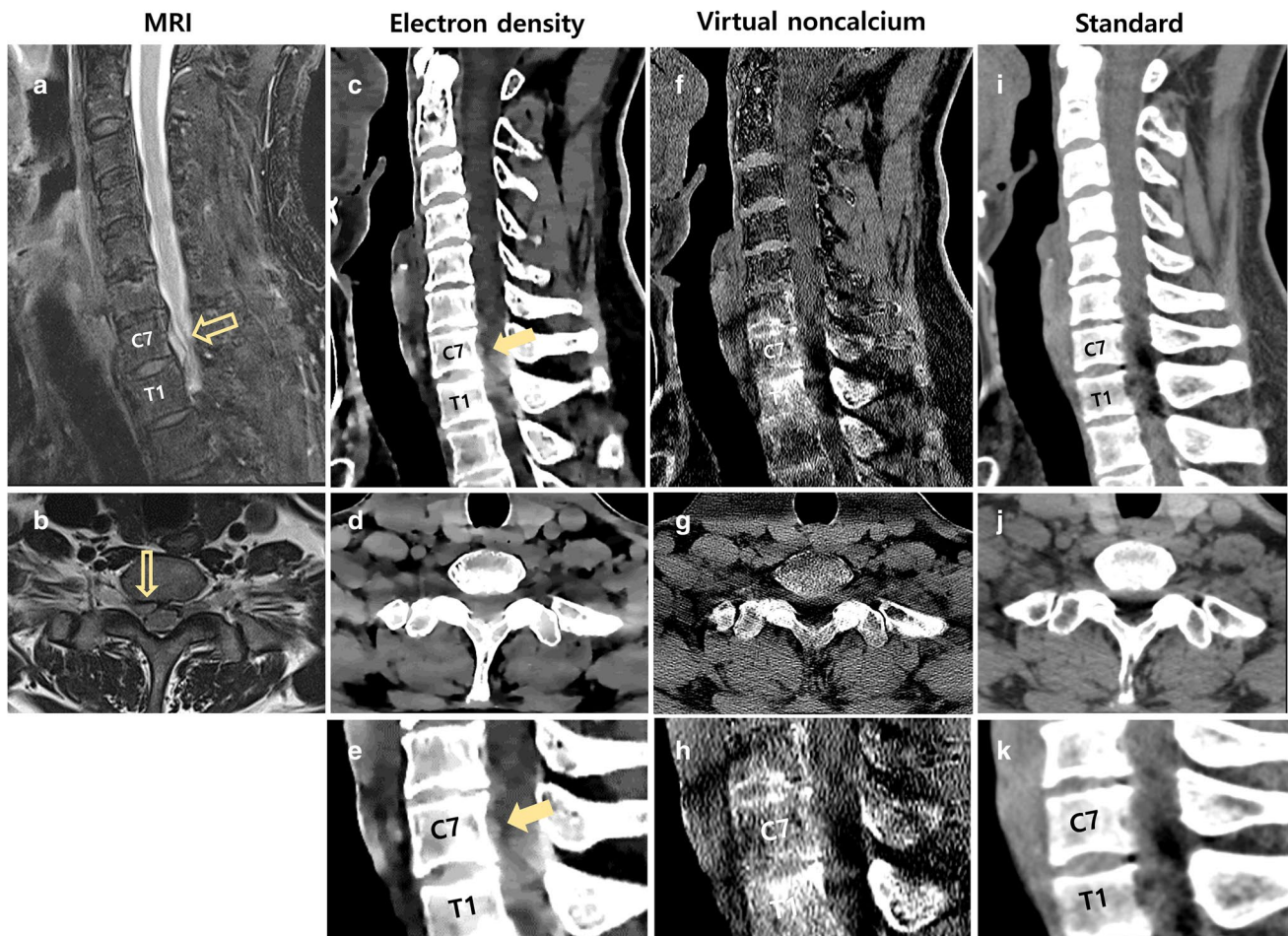
MRI | **Electron density** | **Virtual noncalcium** | **Standard**
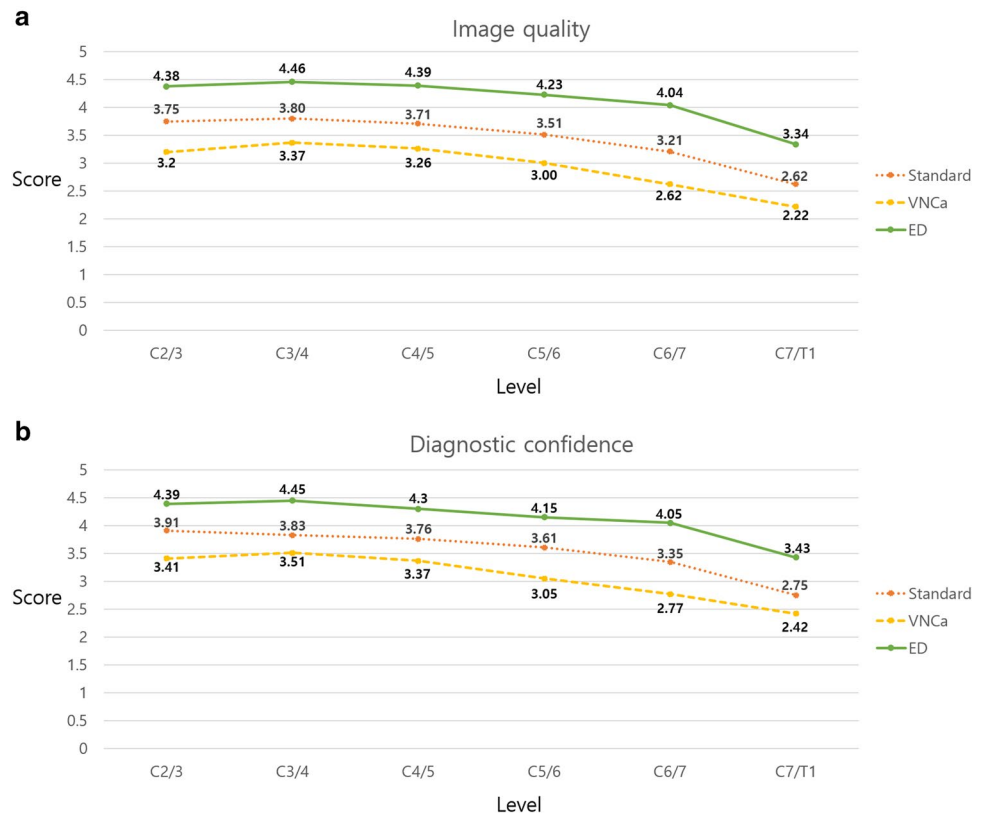
Fig. 5 False-negative case of disc herniation with a high signal intensity on T2-weighted images. A 52-year-old man experienced radiating pain to the right upper extremity. **a**, **b** A superiorly migrated disc at the C7 vertebral body level on fat-suppressed T2-weighted sagittal and non-fat-suppressed T2-weighted axial images (empty arrows). The disc herniation shows a high signal intensity on T2-weighted images. **c–e**, On electron-density images, the migrated disc material is not seen at the C7/T1 disc level (**d**) but partially seen at the mid portion of the C7 body (solid arrows on **c** and **e**). **f–k**, Disc herniation is not observed on virtual non-calcium images (**f–h**) and standard CT images (**i–k**) (**e**, **h**, and **k** are the magnitude views of the lesion). The beam-hardening artifact seems to be aggravated on virtual non-calcium images (**f–h**)

evaluating diseases that occur in organs with very high density (e.g., costal cartilage or discs) and with very low density (e.g., lungs) [8]. Since the contrast between soft tissues is very low on ED images, it may be insufficient to assess diseases in other solid organs.

Herein, VNCa images showed similar sensitivity to SC, unlike the findings for the lumbar and cervical spine reported by Booz et al. [4, 19], who obtained VNCa images by dual-DECT and reconstructed them to obtain color-corded maps using dedicated software. In contrast, we obtained a VNCa map using single-source DECT, and we could not use a color-coded VNCa map because our imaging analysis platform only supported gray-scale VNCa maps. These differences may have reduced the sensitivity of VNCa maps for the detection of disc herniation. In our study, VNCa images tended to be coarse and noisy (Figs. 4 and 5). We thought that the non-color-coded VNCa map showed low image quality since the algorithm used for generating the VNCa map removed the calcium-based material contributing to attenuation of each voxel; therefore, the imaging artifacts not showing calcium-like density may have remained on the map (Figs. 4 and 5) [20]. In contrast, ED maps showed significantly higher subjective image quality than VNCa images with strong noise suppression and increased smoothness in the images in our study [8, 13]. Future studies should aim to compare color-coded VNCa maps and ED maps with/without color-coding.

In our study, 62 of the 64 patients who underwent both cervical spine CT and MRI showed disc herniation at one level or more, and disc herniation was seen in 69.3% of the intervertebral discs (233 of 336). The reported incidence of cervical disc herniation in intervertebral discs varies from
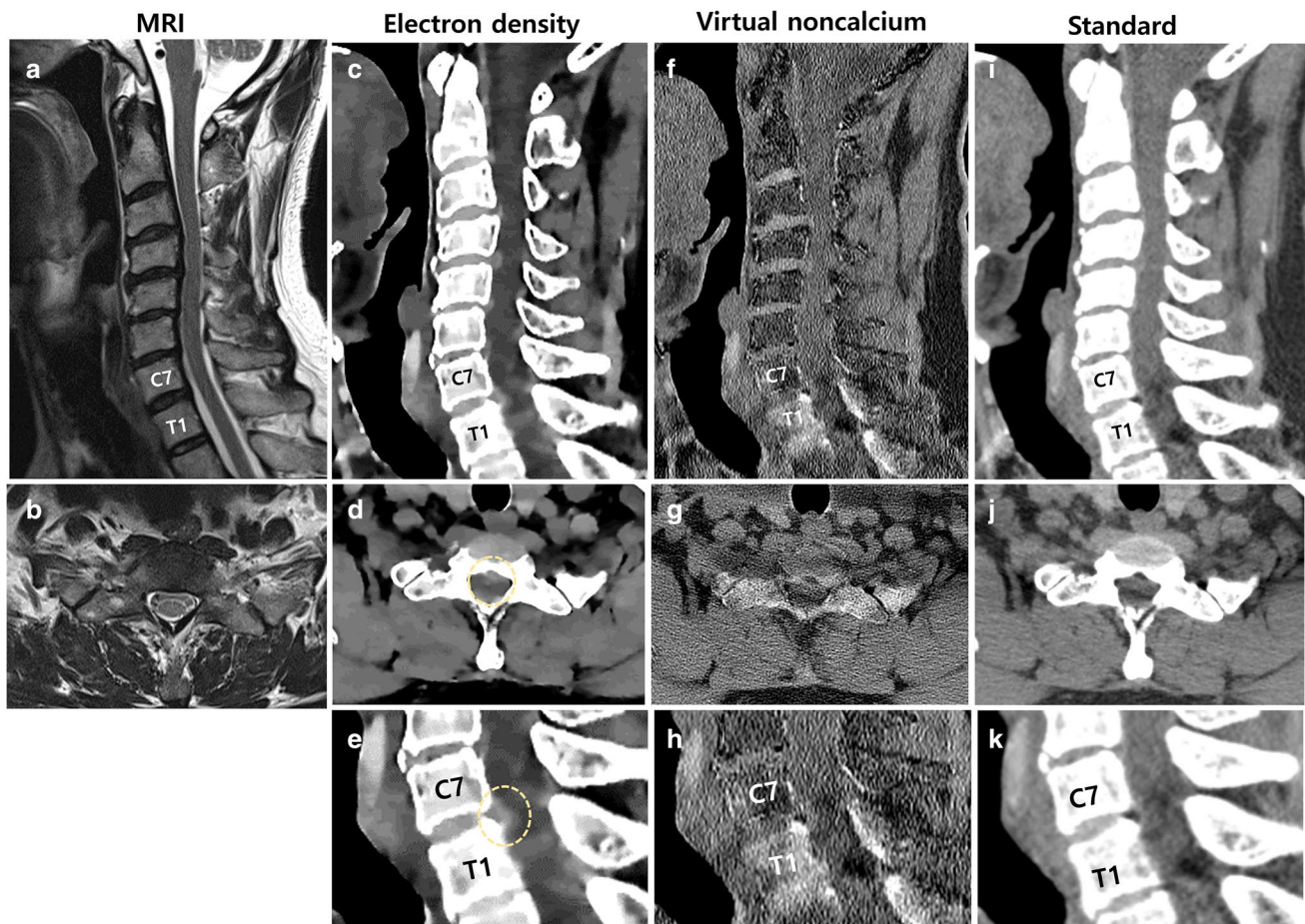
Fig. 6 Pseudo-disc extrusion in a 55-year-old man who underwent cervical MR and dual-energy CT due to right posterior neck pain. **a**, **b** There is no disc herniation at the C7/T1 level on T2-weighted images (**a**, **b**). **c–e**, On electron-density images, disc extrusion appears to be present at the C7/T1 level (dotted circles). **f–k**, Disc herniation is not evident on virtual non-calcium images (**f–h**) and standard images (**i–k**).

27.5 to 67.0% [6, 21]. The high incidence of disc herniation is thought to be the reason why patients usually underwent both CT and MRI in cases of cervical pathology observed in the prior study at our hospital.

The ED map showed 14 false-negative and 10 false-positive intervertebral disc lesions based on the integrated results for the four readers. Non-visualization of two T2 high signal disc herniations on the ED map implies that false-negatives may occur depending on the characteristics of disc herniation. Additionally, the three pseudo-disc extrusions mimicking large herniations at the lower cervical spine suggest that ED values may be miscalculated because of CT artifacts, although the ED map provides noise reduction and more accurate ED values [8, 13].

Our study had several limitations. First, observer variability among readers was high in this study. High observer variability in the assessment of disc herniation is a major concern during study planning [22]. The high observer variability in this study may be related to variable experience levels of the readers, and observer agreement may improve with the availability of a well-organized nomenclature system for the cervical spine. Second, evaluations of three types of images for the same patient may result in recall bias. A completely randomized assessment between imaging methods and patients may be needed to minimize recall bias in future studies.

ED images based on single-energy dual-layered DECT significantly improved the detection of cervical disc herniation and showed increased diagnostic confidence, even at C7/T1. ED images may thus be helpful in diagnosing disc herniation in patients who have undergone only CT scans.

Declarations

Guarantor The scientific guarantor of this publication is Baek Hyun Kim.

Conflict of interest The authors declare no competing interests.

Statistics and biometry Kyung-suk Yang, PhD, has significant statistical expertise.

Informed consent Written informed consent was waived by the Institutional Review Board.

Ethical approval Institutional Review Board approval was obtained.

Methodology
● retrospective
● observational
● performed at one institution

References

1. Beckmann NM, West OC, Nunez DJ et al (2019) ACR Appropriateness Criteria (R) suspected spine trauma. J Am Coll Radiol 16(5S):S264–S285

2. Bischoff RJ, Rodriguez RP, Gupta K et al (1993) A comparison of computed tomography-myelography, magnetic resonance imaging, and myelography in the diagnosis of herniated nucleus pulposus and spinal stenosis. J Spinal Disord 6(4):289–295

3. Notohamiprodjo S, Stahl R, Braunagel M et al (2017) Diagnostic accuracy of contemporary multidetector computed tomography (MDCT) for the detection of lumbar disc herniation. Eur Radiol 27(8):3443–3451

4. Booz C, Noske J, Martin SS et al (2019) Virtual noncalcium dual-energy CT: detection of lumbar disk herniation in comparison with standard gray-scale CT. Radiology 290(2):446–455

5. Lee SM, Choo HJ, Lee SJ et al (2019) Cervical spine CT using spectral shaping: can it be a solution to overcome artifacts in the lower cervical spinal region? Korean J Radiol 20(3):469–478

6. Yi JS, Cha JG, Han JK, Kim HJ (2015) Imaging of herniated discs of the cervical spine: inter-modality differences between 64-slice multidetector CT and 1.5-T MRI. Korean J Radiol 16(4):881–888

7. Hua CH, Shapira N, Merchant TE et al (2018) Accuracy of electron density, effective atomic number, and iodine concentration determination with a dual-layer dual-energy computed tomography system. Med Phys 45(6):2486–2497

8. Daoud B, Cazejust J, Tavolaro S et al (2021) Could spectral CT have a potential benefit in coronavirus disease (COVID-19)? AJR Am J Roentgenol 216(2):349–354

9. Mei K, Ehn S, Oechsner M et al (2018) Dual-layer spectral computed tomography: measuring relative electron density. Eur Radiol Exp 2:20

10. Gupta A, Kikano EG, Bera K et al (2021) Dual energy imaging in cardiothoracic pathologies: a primer for radiologists and clinicians. Eur J Radiol Open 8:100324

11. Raj Arjun S, Chandrashekhara C, Goplani P (2019) Fracture strength estimation of L3–L4 intervertebral disc using FEA. Vibroengineering PROCEDIA 27:67–72

12. ITIS Foundation (2021) Tissue properties. Available at https://itis.swiss/virtual-population/tissue-properties/database/density/. Accessed 22 Mar 2021

13. Simard M, Bar E, Blais D, Bouchard H (2020) Electron density and effective atomic number estimation in a maximum a posteriori framework for dual-energy computed tomography. Med Phys 47(9):4137–4149

14. Brandelik SC, Skornitzke S, Mokry T et al (2021) Quantitative and qualitative assessment of plasma cell dyscrasias in dual-layer spectral CT. Eur Radiol. https://doi.org/10.1007/s00330-021-07821-0

15. Fardon DF, Williams AL, Dohring EJ et al (2014) Lumbar disc nomenclature: version 2.0: recommendations of the combined task forces of the North American Spine Society, the American Society of Spine Radiology and the American Society of Neuroradiology. Spine J 14(11):2525–2545

16 Fleiss JL (1971) Measuring nominal scale agreement among many raters. Psychol Bull 76(5):378–382

17. Landis JR, Koch GG (1977) The measurement of observer agreement for categorical data. Biometrics 33(1):159–174

18. Kanematsu N, Inaniwa T, Nakao M (2016) Modeling of body tissues for Monte Carlo simulation of radiotherapy treatments planned with conventional x-ray CT systems. Phys Med Biol 61(13):5037–5050

19. Booz C, Yel I, Martin SS et al (2021) Incremental diagnostic value of virtual noncalcium dual-energy computed tomography for the depiction of cervical disk herniation compared with standard grayscale computed tomography. Invest Radiol 56(4):207–214

20. McCollough CH, Leng S, Yu L, Fletcher JG (2015) Dual- and multi-energy CT: principles, technical approaches, and clinical applications. Radiology 276(3):637–653

21. Wu Q, Shi D, Cheng T et al (2019) Improved display of cervical intervertebral discs on water (iodine) images: incidental findings from single-source dual-energy CT angiography of head and neck arteries. Eur Radiol 29(1):153–160

22. van Rijn JC, Klemetso N, Reitsma JB et al (2006) Observer variation in the evaluation of lumbar herniated discs and root compression: spiral CT compared with MRI. Br J Radiol 79(941):372–377